GEOLOGICA CARPATHICA, 55, 4, BRATISLAVA, AUGUST 2004
281–298

THE ARCHITECTURE OF THE TROFAIACH PULL-APART BASIN (EASTERN ALPS): AN INTEGRATED GEOPHYSICAL AND STRUCTURAL STUDY

WILFRIED GRUBER[1], REINHARD F. SACHSENHOFER[2], NICOLA KOFLER[3] and KURT DECKER[4]

[1]Institute of Water Resources Management, Joanneum Research, Roseggerstraße 17, 8700 Leoben, Austria
Author for correspondence: Tel: +43 3842 47060 2241, Fax: +43 316 876 9 2241, E-mail: wilfried.gruber@joanneum.at
[2]Department of Geological Sciences, University of Leoben, 8700 Leoben, Austria
[3]Rohöl-Aufsuchungs Aktiengesellschaft, Schwarzenbergplatz 16, 1015 Wien, Austria
[4]Institute of Geology, University of Vienna, Althanstrasse 14, 1090 Wien, Austria

(Manuscript received April 4, 2003; accepted in revised form October 2, 2003)

Abstract: Numerous sedimentary basins including the Trofaiach Basin were formed along wrench corridors during the Miocene lateral extrusion of the Eastern Alps. Because of its rhomboidal outline, a pull-apart mechanism was proposed for the Trofaiach Basin already in the 1980s. However, the internal basin architecture is still widely unknown. To get a better insight into basin formation during continental extrusion, the Trofaiach Basin was studied integrating different geophysical techniques (gravity, seismics, magnetics), digital elevation models, microtectonic and maturity data. Basin formation is related to the E–W trending Trofaiach strike slip fault, which enters the basin at its eastern tip. The northern basin margin is controlled by a terminating branch of this fault, while the main movement was transferred through the basin along subvertical faults in the central basin and along its southern rim. (Oblique) normal faults define the western basin margin. The basin depth reaches a maximum of 800 to 900 m. A fluvial and shallow lacustrine environment was interpreted from seismic facies and borehole data. Clinoform geometries and petrographic evidence indicate sediment supply mainly from the South. Localized coal seams developed in different stratigraphic positions. Water depth probably did not exceed 50 m. Deep lacustrine environments resulting from high subsidence rates are characteristic for many pull-apart basins, but were not established in the Trofaiach Basin. Several erosional events are part of the evolution of the basin. An early erosional phase followed southward tilting of the oldest basin fill and uplift of basement rocks north-west of the basin. A second event caused a major erosional unconformity in the central basin. Finally, related to post-Middle Badenian compression, more than 1 km of strata have been eroded.

Key words: Miocene, strike-slip tectonic, seismic, gravity, magnetic.

Introduction

The Miocene evolution of the eastern part of the Eastern Alps is controlled by lateral extrusion and movement of crustal blocks towards the east (Neubauer 1988; Ratschbacher et al. 1991; Decker & Peresson 1996). The movements occurred along sinistral north-east and dextral south-east trending strike-slip faults. A series of pull-apart basins and half-grabens formed along the Noric Depression, one of the major sinistral strike-slip zones (e.g. Neubauer et al. 2000; Fig. 1).

Mainly because of former coal mining activity, the geology of some Miocene basins along the Noric Depression is fairly well known. In contrast, very little is known about the architecture of the Trofaiach Basin, which does not host economic coal deposits (Weber & Weiss 1983). The main sources of information are coal mines from the turn of the 19th and 20th centuries (Baumgartner, Gimplach; for location see Fig. 2) and three 400 to 550 m deep wells drilled between 1902 and 1951. In spite of the poor knowledge of the basin architecture, the Trofaiach Basin was the first basin within the Eastern Alps for which a pull-apart mechanism was proposed (Nievoll 1985; Neubauer 1988). The main arguments for such a mechanism were the observed sinistral displacements along the Trofaiach Fault and the rhombic shape of the basin.

In the present paper different geophysical methods (reflection seismics, gravimetry, magnetics) together with structural geological investigations are used to reveal the architecture of the basin. Prior to this, unpublished information on the three deep wells and on some recently drilled shallow wells will be presented. Data on the thermal maturity of the basin fill are used to estimate the thickness of eroded rocks. Apart from regional aspects, the investigation should provide better insights into the evolution of small-scale intramontane basins along strike-slip faults.

Geological setting

The Miocene Trofaiach Basin is about 13 km long and up to 5 km wide (Fig. 2). The pre-Neogene basement is formed by the Upper Austroalpine Greywacke Zone, which is composed entirely of Paleozoic rocks (Neubauer et al. 1994). Phyllite and limestone are the prevailing lithotypes with porphyroids, metabasites, and higher grade metamorphic rocks occurring as well. Variscan-Alpine metamorphic rocks of the Middle Austroalpine Unit (gneiss, mica schist, quartzite) are exposed in the southern and eastern study area (Fig. 2).

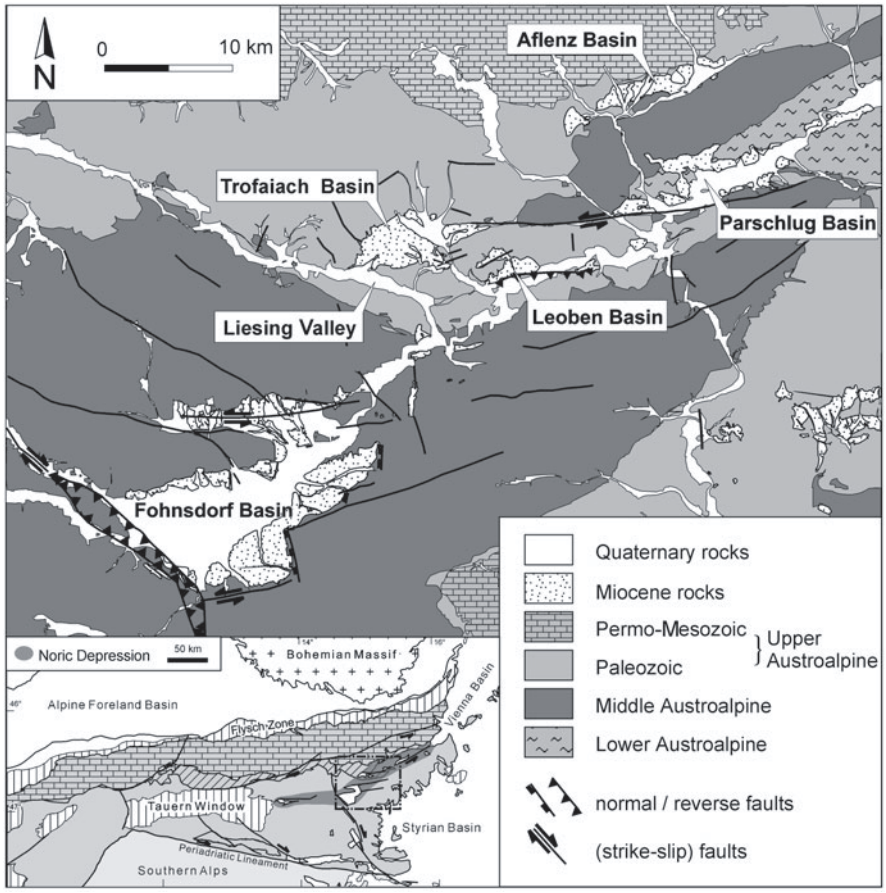

Fig. 1. Sketch map of the study area together with Neogene faults (modified after Decker & Peresson 1996 and Neubauer et al. 2000). The insert shows the study area within the Eastern Alps. The Noric Depression is indicated as a sinistral strike-slip corridor bounding an eastward extruding wedge.

The Trofaiach Basin formed at the western end of the E–W trending left lateral Trofaiach Fault (Vetters 1911), which is part of a system of en-echelon strike-slip faults along the Noric Depression (Metz et al. 1978, 1979). The 30 km long Trofaiach Fault was active in Late Cretaceous times as a ductile shear zone and was reactivated as a brittle shear zone during Miocene times (Neubauer et al. 1995; Nievoll 1985).

Due to limited exposures, the basin fill and its internal structure are poorly known. According to Petrascheck (1924), flat lying reddish conglomerates interlayered by clay and red paleo-soil north-west of Trofaiach represent the oldest rocks. Except for this area, the basin fill generally dips towards the south-east and is dominated by shale, sandstone, and thin conglomeratic layers. Tuffitic horizons are also present. The bedding dips at higher angles (up to 30°) along the north-western basin margin and is lower (about 10°) near the fault controlled southern margin of the basin. Gently westward dipping sandstones were observed in the basin centre (Hoefer 1902a).

Thin SSE dipping (~25°) coal seams occur in a deep stratigraphic position near Baumgartner ("lower seam") and in a higher position near Gimplach ("main seam"; Hoefer 1902a). The "lower seam" is accompanied by sapropelic shale with numerous shells. The "main seam" consists of two coal beds each about 1 m thick separated by a shaly and sandy succession. Hoefer (1902a) mentioned an "upper seam" a few hundred meters above the "main seam". Thin coal seams in even higher stratigraphic positions are known to exist in different parts of the Trofaiach Basin.

A tuff layer in borehole A5 (252 m above sea level) was dated using the zircon fission track technique and yielded an age of 17.3±1.2 Ma (I. Dunkl, pers. comm.). This indicates that the basin fill has a similar age to that of neighbouring Karpatian (late Early Miocene) to Badenian (early Middle Miocene) basins along the Noric Depression (e.g. Sachsenhofer et al. 2000; Weber & Weiss 1983).

Borehole data

Lithologs of the boreholes Dirnsdorf, Trofaiach 1, Trofaiach 2, KB1–3 and A5 are shown in Fig. 3. Unfortunately none of the boreholes was further investigated by wireline logs.

Very little is known about the 150 m deep borehole Dirnsdorf, which drilled through two thin seams at 27 m (0.65 m thick) and 48 m (0.45 m) depth. Although the drill site is located only about 300 m from the western basin margin, it did not reach the basement.

Trofaiach 1 investigated the sedimentary sequence beneath the "main seam" horizon near Gimplach (Hoefer 1902a). It

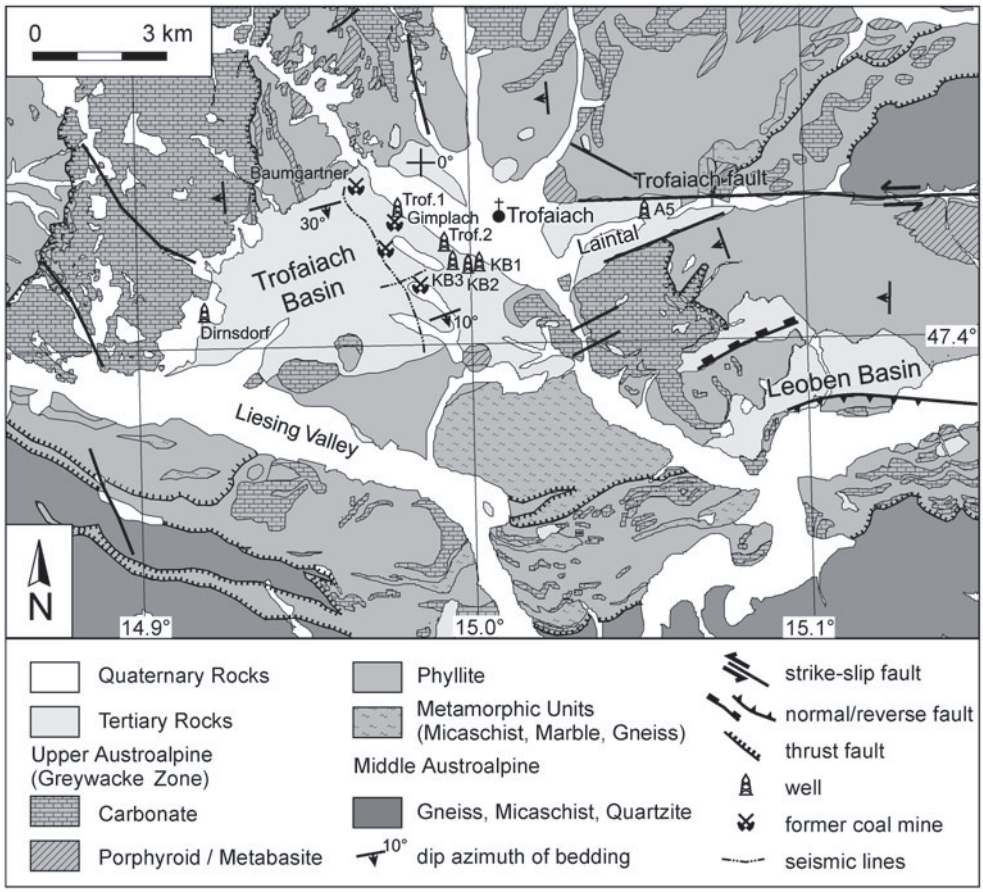

Fig. 2. Simplified geological map of the study area showing well locations and former coal mines within the Trofaiach Basin.

drilled mainly shale, coaly shale, several thin layers of sandstone and reached the phyllitic basement at a depth of 450 m. Trofaiach 2 was planned to investigate the succession above the "main seam" and penetrated shale, some coaly shale, a seam 0.3 m thin in 196 m depth and several layers of sandstone and conglomerate (Hoefer 1902). Gas eruptions (methane?) were reported at depths of 268 m (conglomerate) and 280 m (shale; Weber & Weiss 1983).

Boreholes KB1 to KB3 are located near the basin centre and drilled grey sandstone, siltstone and claystone. A number of fault planes, either with horizontal slickenside lineation or with steeply dipping vertical lineations, were penetrated in KB1 and KB2.

Borehole A5 is located in the narrow Laintal Valley and is 555 m deep (Lackenschweiger 1951). Nevertheless the basement was not reached, clearly indicating steep basin margins. The sedimentary succession is dominated by shale, calcareous shale and sandstone. In comparison to boreholes Trofaiach 1 and 2 in the central basin, the proportion of sand is higher in A5. Two tuff horizons more than 1 m thick and a few thin layers of coal and coaly shale occur as well. Conglomerates near the base of the borehole were interpreted as representing a basal conglomerate. The drilled rocks are generally gently dipping (10–20°), but are steeper in a heavily faulted zone between 437 and 452 m depth. A steeply dipping calcite filled fault was penetrated in 430 m depth (see insert in Fig. 3). Left lateral motion was reconstructed from fibrous calcite observed in drill cores.

Thermal maturity

Vitrinite reflectance of surface samples and samples from wells A5 and KB1–3 were determined following established procedures (Taylor et al. 1998). Results are presented as random reflectance values (R_r). Additional data were taken from Sachsenhofer (1989).

Vitrinite reflectance in well A5 decreases upwards from about 0.55 to 0.40 % R_r. In spite of the rather short depth interval and the scatter of the data (Fig. 4), the reflectance trend was used to estimate the thickness of eroded rocks. In a first attempt linear and logarithmic trend lines were calculated and extrapolated to a surface value of 0.2 % R_r. The results suggest that rocks 1000 m to 1500 m thick were removed above the youngest outcropping sediments. The basin modelling approach was also applied, using PetroMod 1D software (Yalcin et al. 1997) and the subsidence history shown in the insert of Fig. 4. A good fit is obtained assuming a paleoheat flow of 85 mW/m^2 and erosion of rocks 1200 m thick. Note that the short depth interval results in a considerable uncertainty of the heat flow estimate (±25 %). However, an elevated heat flow in the Trofaiach area fits well with paleoheat flow maps for Miocene times (Sachsenhofer 2001).

Along a surface profile in the central Trofaiach Basin, vitrinite reflectance increases from 0.32 % R_r in the northwest (Baumgartner) to 0.41 % R_r in the south-east (Fig. 4). Even higher values occur in the Leoben Basin. Within the

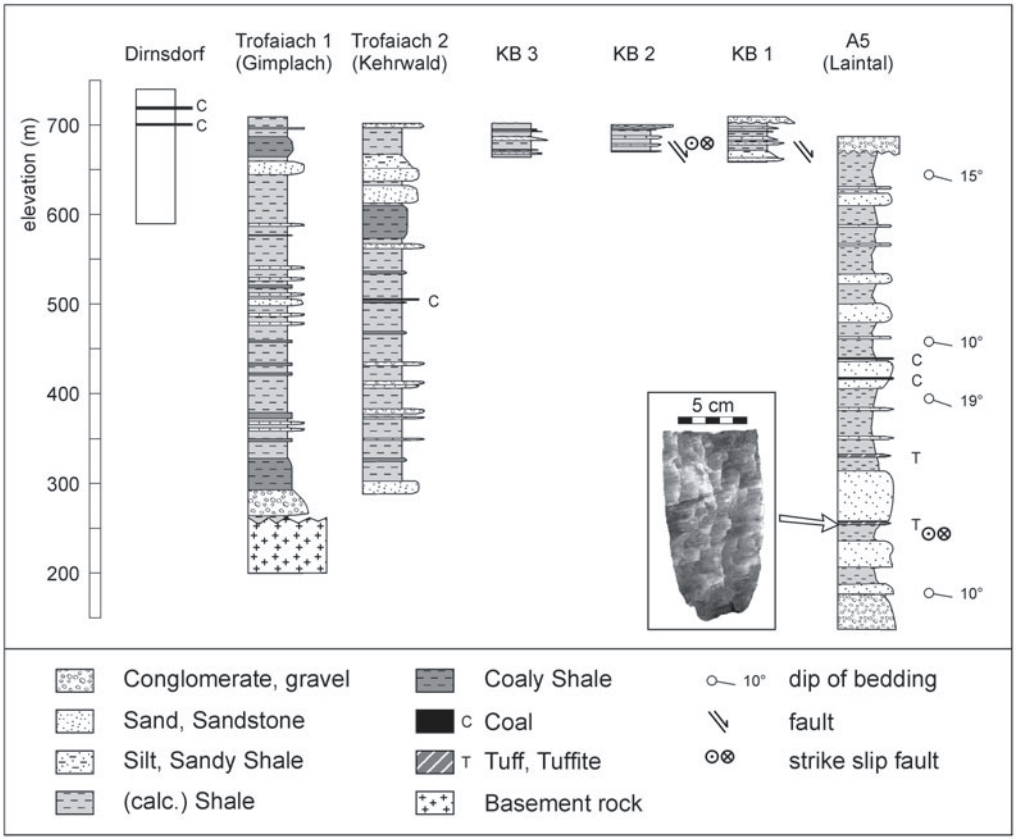

Fig. 3. Lithostratigraphic profiles of boreholes in the Trofaiach Basin (after Hoefer 1902a,b; Petrascheck 1924; Lackenschweiger 1951). For location see Fig. 2. Insert shows a photograph of fibrous calcite indicating post sedimentary sinistral movements along the Trofaiach Fault.

Trofaiach Basin the oldest sediments are exposed at the northwestern basin margin and are characterized by the lowest reflectivity. This suggests that the south-eastward increase in maturity is controlled by lateral heat flow variations rather than by the stratigraphic position of the rocks (see also Sachsenhofer 2001).

Geophysical investigations

A published Bouguer gravity map of Styria includes the Trofaiach Basin (Winter 1993), but is not detailed enough for this study. Therefore, in a first step, the resolution of this survey had to be improved by measuring additional gravity stations. Preliminary results of the gravity survey were used to find the best location for two reflection seismic profiles. Additional gravity data were acquired along the main seismic profile. Finally, a magnetic survey was conducted. The primary aims of the latter were to support the interpretation of the gravity data and to track the strike of fault planes interpreted in the seismic section.

Reflection seismic lines

Data acquisition and processing

In May 2000 two shallow reflection seismic lines were acquired. The locations of the seismic sections are shown in Fig. 2. The NNW–SSE directed profile TR0001 is 4 km long. It starts about 250 m south of the northern basin margin, crosses the depocenter of the basin, and ends at the southern basin margin. Spacing of the receiver stations was fixed to 10 m and an accelerated drop weight was the seismic source.

Data processing was performed on a Unix based workstation by using the Focus/Disco software package and followed standard procedures for land seismic data. Wave equation migration was performed on line TR0001 using a velocity model slightly faster (105 %) than the stacking velocity. The final display of time sections refers to a datum plane of +650 m above sea level.

Seismic interpretation

The PC based SeisX software package was used for geological interpretation. Interpreted horizons are denoted in capital letters (A–H), faults are labelled by numbers (1–5). The stacking velocity was used for rough depth estimations. Interval velocities calculated from stacking velocities are 2100 to 2500 m/s for upper complex rocks, 2700 to 3200 m/s for lower complex rocks and above 3800 m/s for basement rocks.

On line TR0001 good information above the pre-Miocene basement is provided only along the northern part of the transect, where it is represented by a southward dipping baselap surface. The phyllitic basement is characterized by low reflectivity. The position of the top of the basement is fur-

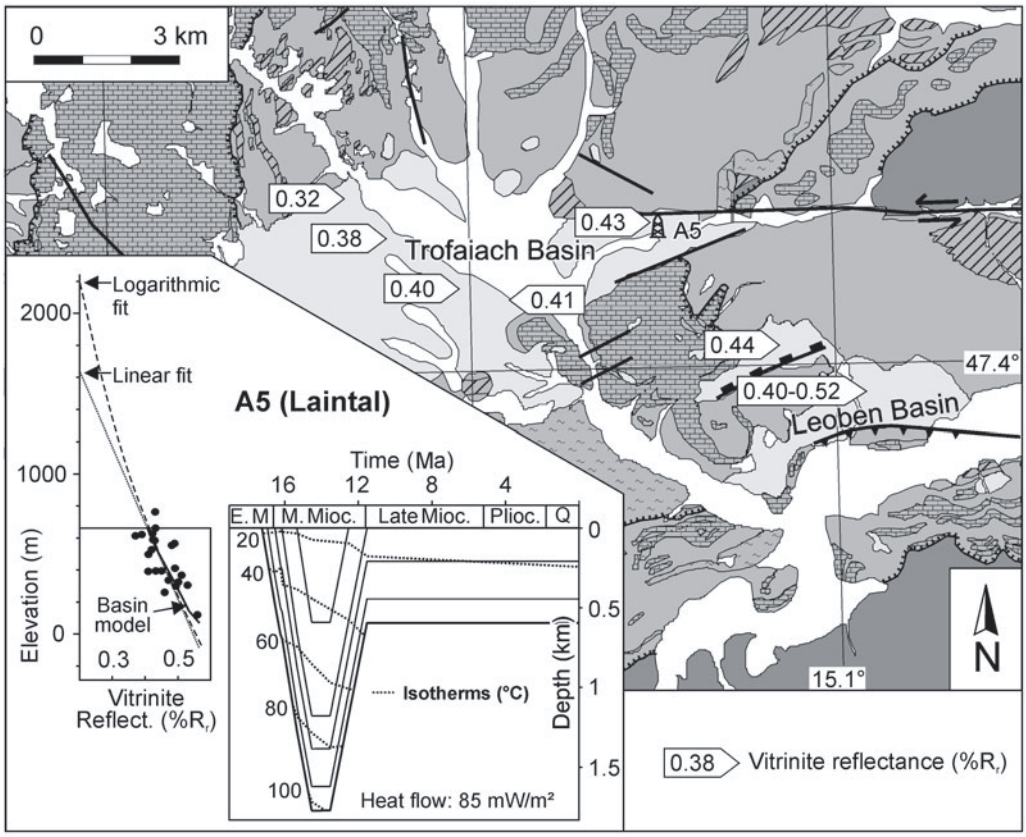

Fig. 4. Vitrinite reflectance in the Trofaiach and Leoben Basins. Insert shows vitrinite reflectance in well A5. Linear and logarithmic trend lines are extrapolated to a "surface value" of 0.2 % R_r. Its elevation suggests erosion of rocks 1000 m or 1500 m thick. A basin model, assuming the subsidence history shown and a heat flow of 85 mW/m^2, results in 1200 m of missing rocks.

ther constrained by exposures near the northern end of the seismic line and by well Trofaiach 1, which penetrated the basement at a depth of 450 m. In contrast to the north-western basin margin, the southern margin is formed by steep faults. This interpretation is supported by exposures of basement rocks south of station 480. The interpretation of the basin configuration between stations 320 and 460 is ambiguous. The absence of reflections below 500 m suggest a small horst at station 380 which separates horizontal reflections of the depocenter in the north from southward dipping reflectors in the south. However, the exact basement depth is unclear. The Miocene basin fill is subdivided into a *lower complex* and an *upper complex* by horizon E.

The seismic facies of the *lower complex* differs greatly along the transect. At the northern transect southward dipping reflectors generally exhibit a high amplitude. The deepest reflectors terminate against the basement in a baselap relation. Reflectors below horizon B show lapouts on either side. This reflection geometry indicates sediment transport oblique to the transect. Conglomerates, shales and coaly shales in the deepest part of well Trofaiach 1 suggest deposition in a fluvio-deltaic environment. Horizons C and D enclose a northward prograding sedimentary package characterized by downlaps. Clinoform geometries indicate a water depth in the order of 50 m. Sediments below an elevation of 500 m in Trofaiach 1 which show a coarsening upward trend possibly represent this interval. Several northward dipping listric faults ((1) in Fig. 5) displace the basement and the lower part of the basin fill south of station 175. The faults cannot be traced to the surface and were obviously only active during early stages of basin formation. Despite faulting and significant lateral variations in the thickness of single horizons, the thickness of the complex between the top of the basement and horizon D is quite uniform. This suggests that the top of the basement was not yet tilted during deposition of the rocks beneath horizon D. Thereafter, normal faulting along the prominent fault 2 rotated the lower part of the lower complex. The accommodation space created by faulting was filled by sediments baselapping against horizon D. It cannot be decided whether it is an onlap relationship or the downlap of northward prograding clinoforms. In the latter case, the topset area is dislocated by fault system 3. The upper part of the lower complex is characterized by a lower dip angle than that below horizon D. This is due in part to faulting along the listric fault 2. However, an effect of fault 3, which might have re-rotated the higher part of the lower complex, cannot be excluded. Along the central and southern part of the seismic section, facies interpretation of the lower complex is problematic due to the absence of continuous reflectors. Perhaps the rather chaotic low amplitude reflectors result from intense strike-slip faulting. Horizons F and G define the base of the sequences with northward prograding clinoforms near the southern basin margin. It cannot be decided, whether these horizons correlate with horizons C and D at the northern basin margin.

Before deposition of the *upper complex*, major erosion caused erosional truncations between stations 330 and 380

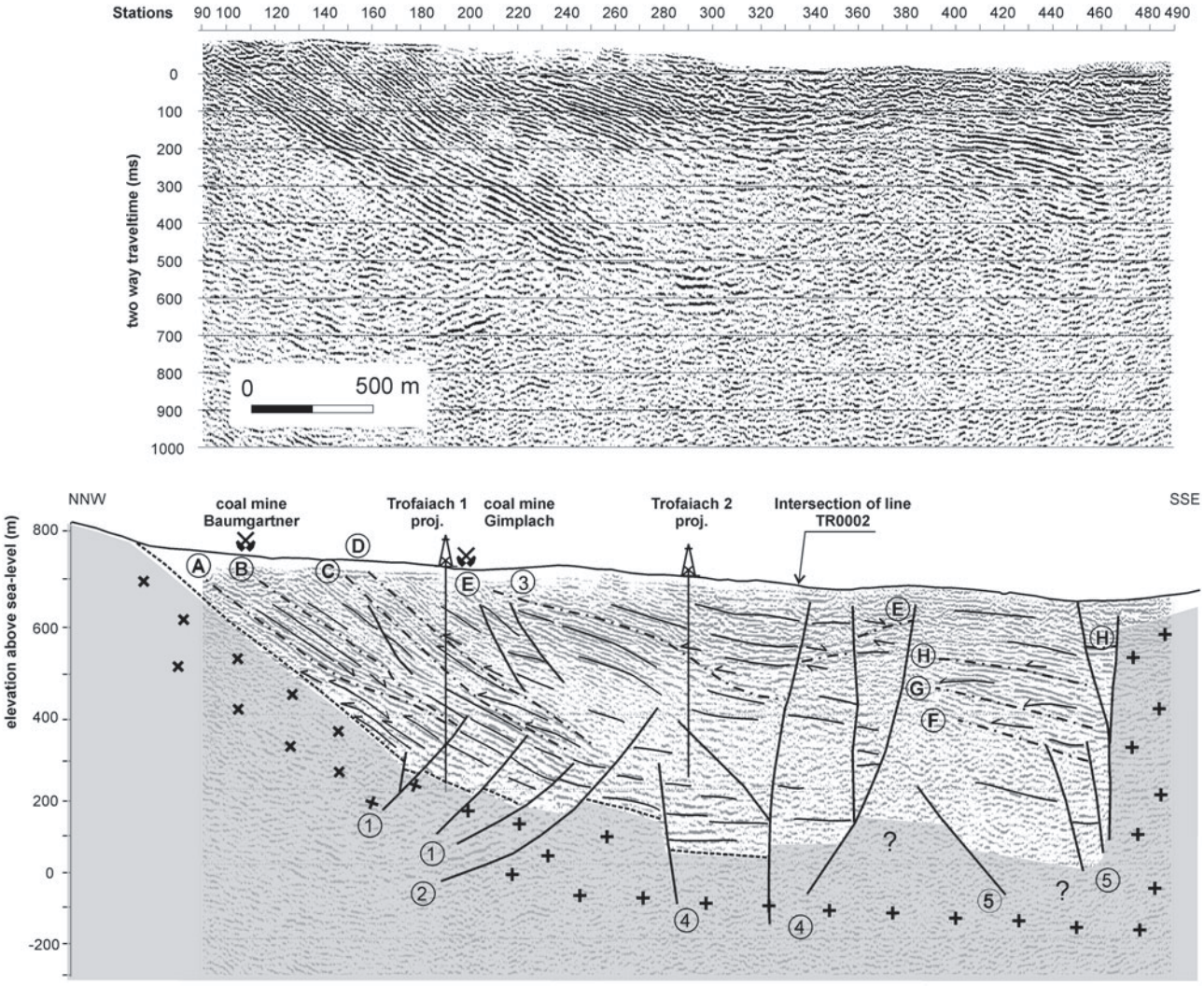

Fig. 5. Migrated seismic time section (above) and interpretation of the NNW–SSE profile TR0001. Nonlinear depth scale is estimated from stacking velocities and refraction analyses. Well projection distances are 630 m for Trofaiach 1 and 1100 m for Trofaiach 2. Faults are referenced by numbers, main horizons by capital letters.

and created a prominent reflector (horizon E). The resulting relief was filled up by the upper complex onlapping the erosional surface. Reflectors are generally characterized by a low continuity and moderate amplitude. Upper complex sediments dominated by shale and sand were drilled by boreholes KB1–3 and Trofaiach 2. Thin coal seams are present in outcrops and KB boreholes, suggesting a similar depositional environment to that during deposition of the lower complex. Fault systems 4 and 5 reach the surface and displace horizon E and upper complex sediments. Obviously, these fault systems are younger than faults systems 1 and 2. Tectonic data from boreholes KB1 and 2 suggest a major strike-slip component of fault system 4. Fault system 5 corresponds to the south-eastern basin margin.

Line TR0002 is of bad data quality due to unfavourable positioning parallel to the main fault zone. Some information comes from the uppermost 200 m, where reflectors of low coherency show slight westward dips. Further detailed interpretations are impossible.

Gravity survey

Data acquisition and processing

250 gravity stations were measured using a LaCoste-Rhomberg gravity meter model G 374. Data collection was performed in a single loop measurement with multiple instrument readings. The altitude of the gravity stations was determined by differential-GPS surveys with an elevation error ranging from 1 to 10 cm.

Data processing started with tidal corrections, which indicated small long-term drift rates. Subsequently the Bouguer corrections and terrain corrections to a reference spheroid were made. Fay's and Bouguer corrections were done for a correction level of +600 m and simply a constant reduction density of 2670 kg/m^3. In order to represent the data graphically the irregularly spaced grid must be interpolated. In geostatistical analyses of the processed data an anisotropy for the directional angle of 33° with an axis ratio of 1 : 2 was ob-

served. A Kriging algorithm utilized these results in a variogram model, which was used for gridding.

In the contour map of the Bouguer anomaly (Fig. 6a) the values range between –25.9 mGal and –9.6 mGal. The correlation between gravimetric and topographic structures indicates that surface effects predominate the anomaly field. For further structural enhancement of the anomalies a regional field was subtracted from the Bouguer data. This regional field was defined by a simple first order polynomial. The obtained residual anomaly map is not shown, since it displays similar features to the Bouguer anomaly map. The horizontal gradient of the Bouguer anomaly is mapped in Fig. 6b. The gradient of the Bouguer anomaly highlights zones of maximum lateral changes in gravity and thus traces the boundary between bodies of different densities. This can be caused either by fault related basement relief or by anomalies within the basement or basin fill.

The basin structure was modelled along seismic line TR0001 using the residual gravity field for calibration. The model calculation was carried out using the program GM-SYS. The main goal of the model is to check whether the basin structure interpreted from the seismic line is in accordance with observed gravity data.

Interpretation

Gravity field

The Bouguer anomaly outlines the overall shape of the basin as an elongated flat bottomed trough (Fig. 6a). The central parts of the basin are characterized by the most negative values (–26 mGal to –22 mGal). The basin depth appears to be constant in the western and central parts and shallower in the narrow eastern part.

The gradient map (Fig. 6b) yields information on the location of faults. A WSW–ENE trending zone with very high gradients follows the steeply dipping south-eastern basin margin fault. Another zone with a high gradient represents a parallel lineament north of the basin margin. The gradient along this fault increases towards the south-west. This is probably because the lineament is a central basin fault in the east, which grades into the basin margin in the south-west. Both faults were interpreted along seismic line TR0001. The southern fault corresponds to fault system 5, whereas the northern fault was labelled fault system 4.

Due to a low number of gravity stations in the north-eastern study area, the trace of the Trofaiach Fault in the Laintal area is hardly reflected in the gravity maps. However, the continuation of the Trofaiach Fault west of Trofaiach is visible as a roughly E-W striking zone with a high horizontal gradient. Note that the western segment of the Trofaiach Fault is not exactly the continuation of the fault forming the northern basin margin in the Laintal area. This suggests subtle displacements of this major strike-slip fault.

Two NE–SW oriented segments with high gradients occur at the north-western basin margin. Because of a low density of gravity stations in this area (Fig. 6a), the exact position of the southern segment is poorly constrained. The most eastern position theoretically possible is shown in Fig. 6b. Even in this case, the pattern of gravity anomalies suggests that the western basin flank is displaced along an E–W trending line.

Model results

The gravimetric model along seismic line TR0001 is shown in Fig. 7. Bench marks of the basin geometry are a shallow dipping north-western basin flank constrained by seismic data, borehole Trofaiach 1 and a nearly vertical southern basin margin.

Laboratory measurements of 15 phyllitic basement rocks yielded an average density of 2690 kg/m^3. The average density of Paleozoic carbonates beneath the Styrian Basin is 2770 kg/m^3 (Sachsenhofer et al. 1996). Considering these results, a model density of 2720 kg/m^3 was used for the mainly phyllitic basement. Hussain & Walach (1980) determined in situ density values for Miocene sandy marls (2520 kg/m^3) and sandstones (2630 kg/m^3) in the nearby Fohnsdorf Basin (see Fig. 1 for location of Styrian Basin and Fohnsdorf Basin). On the basis of this work, and in order to underestimate rather than to overestimate basin depth, a density of 2520 kg/m^3 was adopted for the deeper parts of the Miocene basin fill and 2450–2480 kg/m^3 for the shallower parts of the basin fill.

Upward decreasing densities of the sedimentary basin fill can be related to lower compaction rates of shallower layers. Both, the 2450 kg/m^3 body in the northern part and the 2480 kg/m^3 in the southern dip parallel to the bedding planes and are structured by the main faults (Fig. 7). The high gravity gradient near profile meters 2000 and 3900 suggests a shallow depth for a body with significantly lower density. This body might partially represent *upper complex* rocks.

The deeper structure of the southern part of the basin is more speculative, so two alternative models with comparable residual error were tested. Model A follows the seismic interpretation where the basement is characterized by a horst. Model B incorporates a broad depocenter, a sub-horizontal basement top, but a higher density of the sedimentary sequence.

Magnetic survey

Data acquisition and processing

The total magnetic intensity (TMI) was measured along 7 profiles (Fig. 8) with an overall length of 21.5 km. Readings were made at a station spacing of 30 m using a Geometrics G816/826 proton magnetometer. The readings were repeated three times and subsequently averaged at every station. Stations close to powerlines, buildings, known pipes and those with larger fluctuations than ±2 nT were rejected. Station coordinates were obtained to within 5 m by using a portable GPS receiver. Data processing included corrections for diurnal variations recorded at a base station every hour and for latitude (0.0026 nT/m), longitude (0.001 nT/m) and elevation (–0.02 nT/m) referred to the base station (Militzer & Weber 1984).

Kriging, using variogram analysis, provided a TMI database to derive a contour map (Fig. 8). Profile spacing is large compared to the station intervals so that only regional features can be interpreted on the contour map. Interpretation of high frequency anomalies can only be performed along a measured profile.

In addition, a 2.5 D modelling technique was used to derive models with bodies causing the main magnetic anomalies

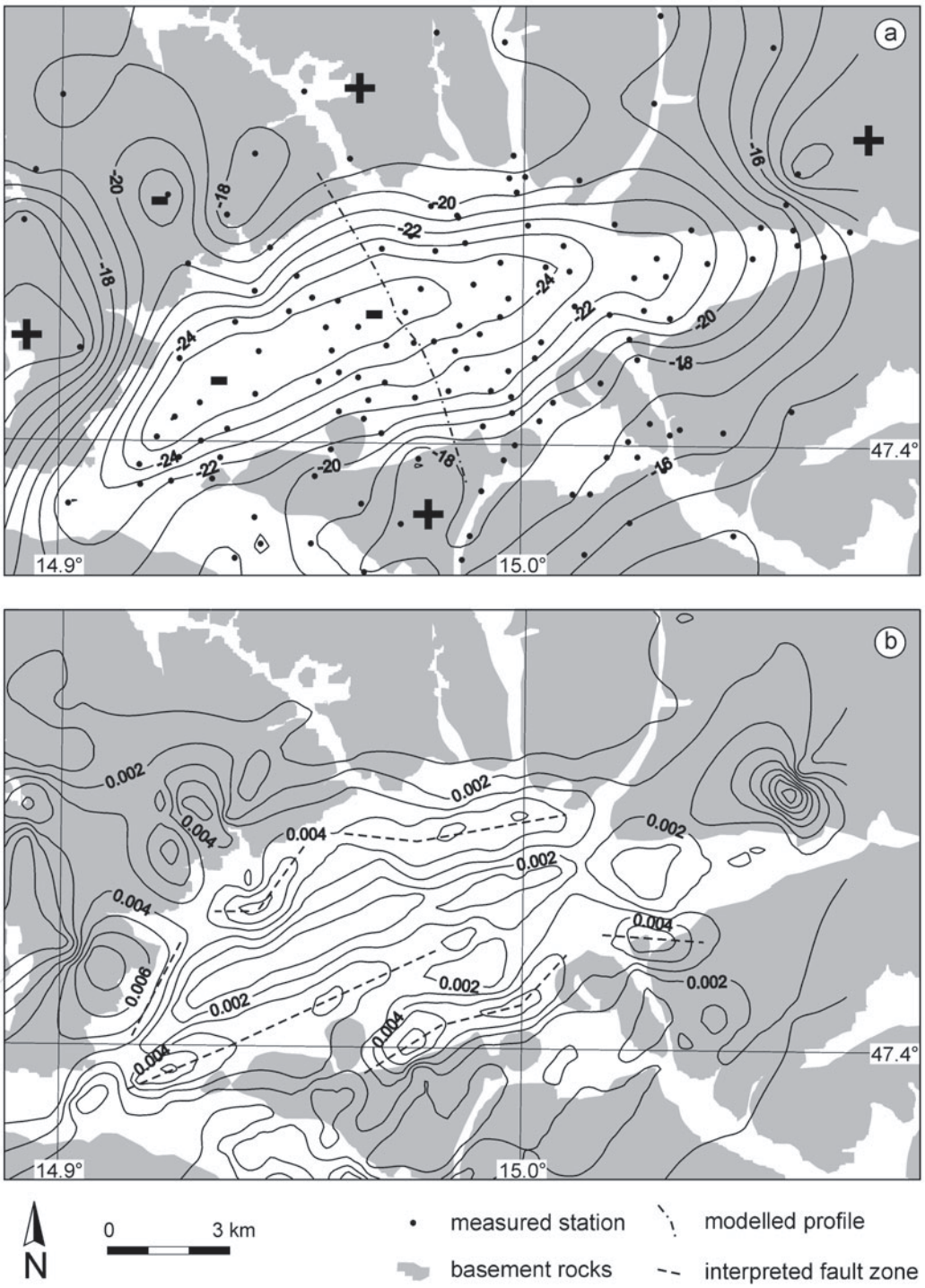

Fig. 6. a — Contour map of Bouguer anomaly in mGal at a correction level of 600 m above sea level. Dots indicate the stations measured. **b** — Contour map of the first derivative calculated from the Bouguer anomaly. Lines indicate zones with high gradients interpreted as major fault zones.

along the profiles. For this, a linear regional field has been subtracted from the measured data. The models were calibrated by comparing the calculated magnetic patterns with the residual field. Susceptibilities were determined on hand picked samples by Ströbl (pers. comm.) yielding a mean value of 0.001 SI units for limestone and 0.005 SI units for phyllite and gneiss. Higher values (0.015 to 0.8 SI units) were obtained from the porphyroid and metabasite samples.

Interpretation

TMI field

The total magnetic intensity ranges from 47700 to 48100 nT except at the northern end of profile 3, where drinking water reservoirs cause major disturbances (Fig. 8). There is an overall southward decrease in TMI. This is the marginal

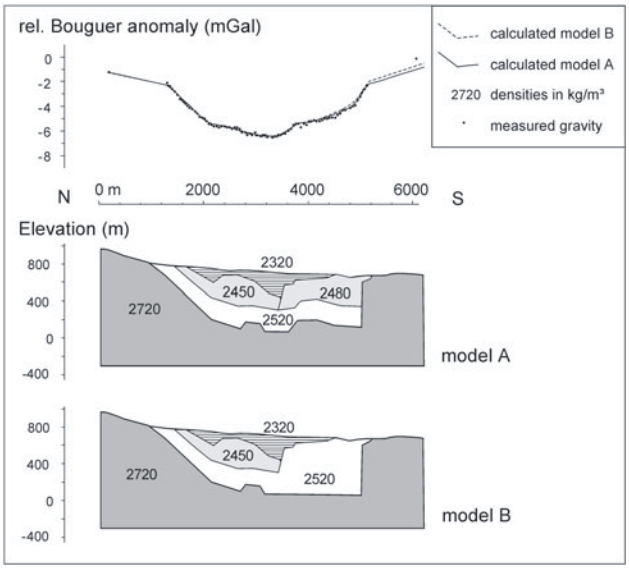

Fig. 7. 2.5 D gravity modelling along the profile shown in Fig. 6.

effect of a giant positive anomaly (+700 nT, 8 km wavelength) located north of the Trofaiach Basin (Gössgraben anomaly according to Ströbl, pers. comm.). Within the study area, major, mostly positive anomalies define areas with shallow or outcropping basement, whereas a generally smooth magnetic pattern occurs in the central basin. The smooth character of the magnetic field within the Trofaiach Basin is disturbed only by small-scale negative anomalies of 10 to 30 nT amplitude and 100 to 300 m wavelength (Fig. 9). Benson & Mustoe (1995) report that negative anomalies may be due to oxidation and alteration of magnetite and secondary deposition of limonite by ground water moving through fault zones. This interpretation agrees with the observation that the southern basin margin fault is characterized by negative anomalies.

Model results

Several profiles cross the southern basin margin. Model bodies with a susceptibility contrast of about 0.003 SI units relative to the basin fill have to be considered to fit the observed magnetic data at the southern parts of profiles 6, 4 and 3. The body at profile 6 reaches the surface and correlates excellently with exposures of porphyroids at the southern end of this profile (Fig. 2). The model bodies at profiles 6 and 4 have vertical northern edges indicating truncation by steep faults, which cause small negative anomalies. Towards the east (profile 2), the models suggest the presence of a structured body with a relative susceptibility of 0.002 SI units, representing a shallow, faulted basement. The faulted basement probably extends eastwards to the southern part of profile 1 characterized by strong variations in the magnetic field. A distinct TMI decrease at the very southern end of profile 1 indicates a body with a lower susceptibility (–0.002) than the basin fill. Comparable low susceptibilities were measured by Ströbl (pers. comm.) in carbonates exposed at the southern end of profile 1 and at the western basin margin (Fig. 2).

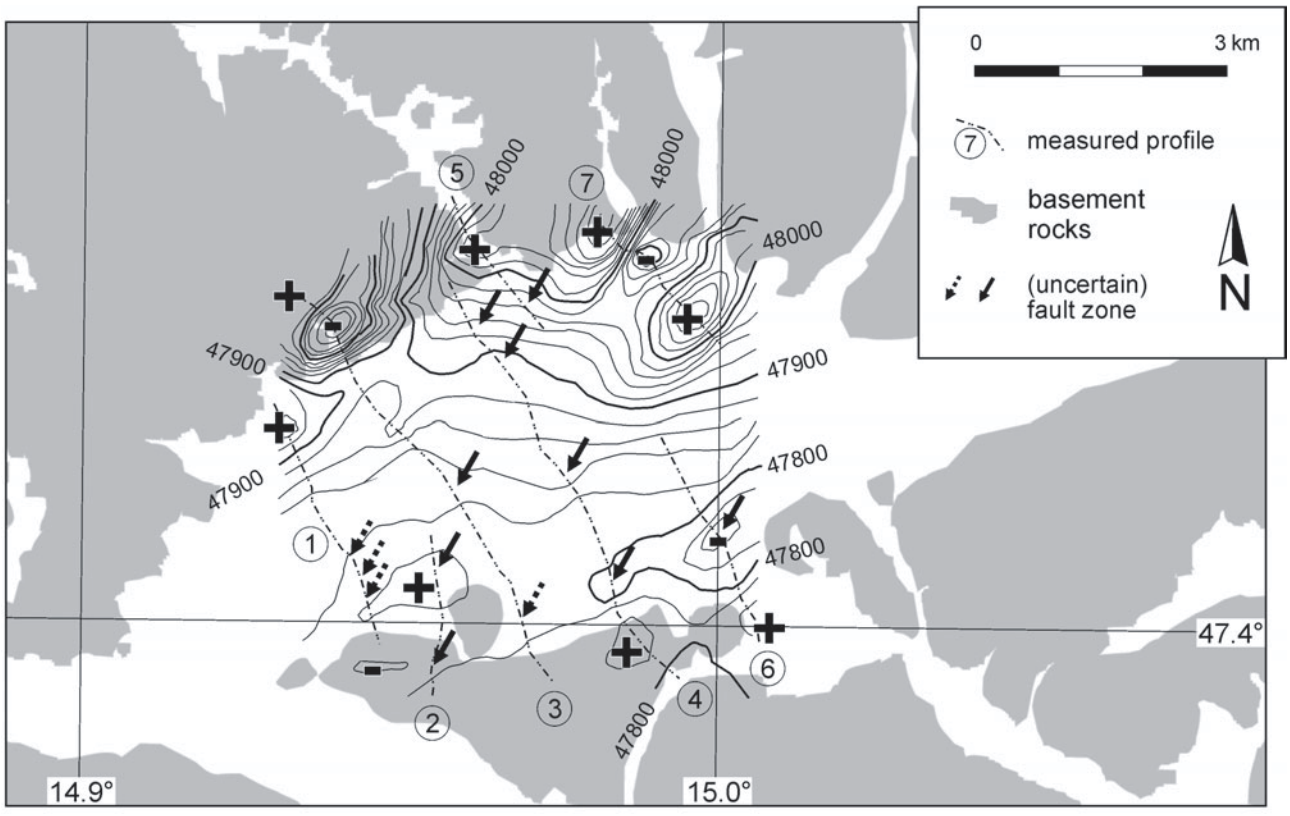

Fig. 8. Map of total magnetic intensity in nT measured along the profiles shown. Arrows indicate local negative anomalies interpreted as fault zones, "+" and "–" signs indicate regional positive and negative anomalies.

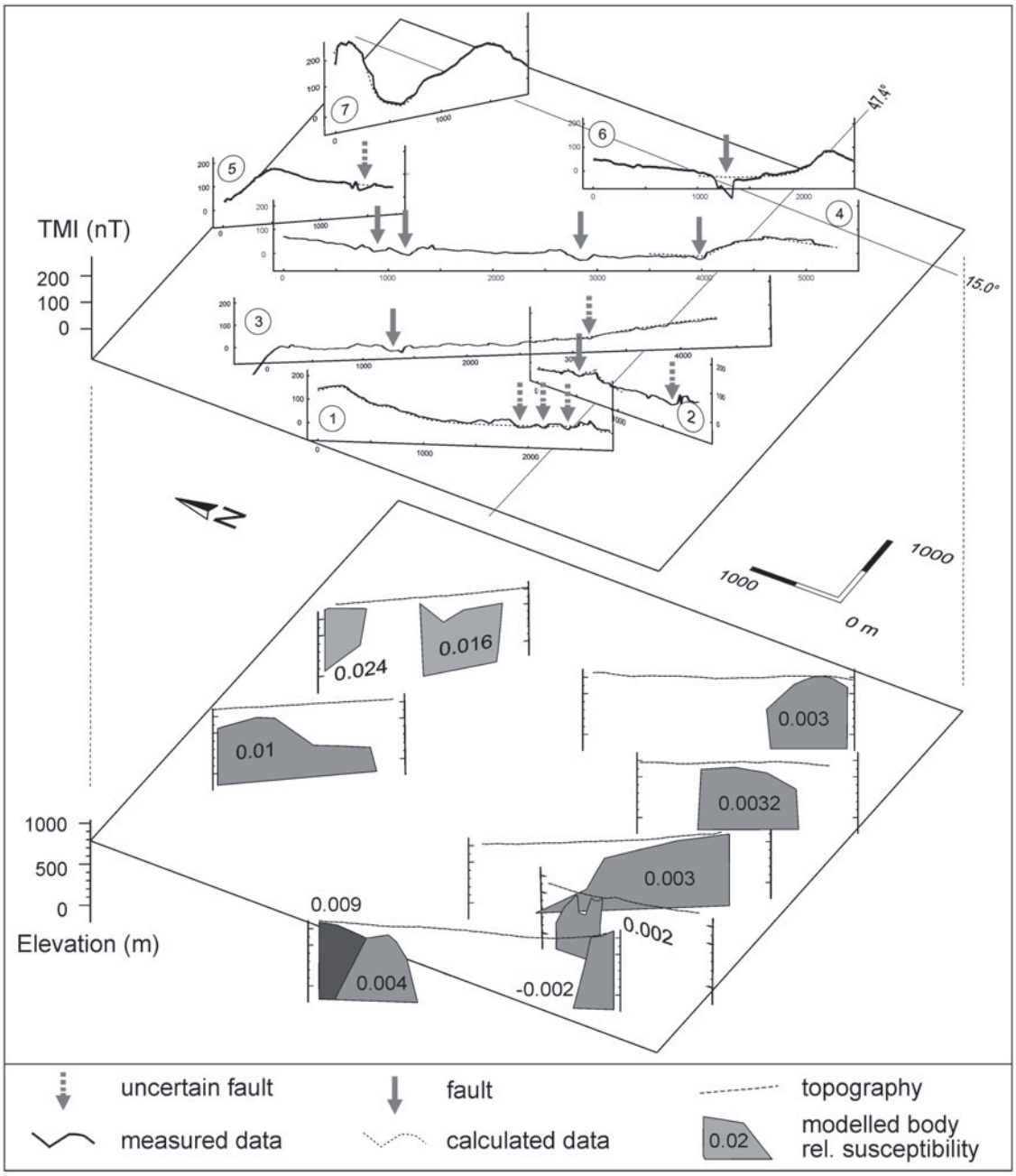

Fig. 9. A perspective view of relative total magnetic intensities along seven profiles is shown in the upper part. Arrows point to anomalies with a short wavelength interpreted as fault zones. Modelled bodies causing the observed long wavelength anomalies are shown in the lower part. Numbers denote relative susceptibility in SI units. See Fig. 8 for position of profiles.

Information about the northern and western basin margins is provided by profiles 7, 5 and 1. High susceptibilities (0.024 and 0.016) have to be assumed for shallow bodies along profile 7. These bodies are probably related to metabasitic rocks, which are exposed east of the profile, north-east of Trofaiach. This interpretation points to a shallow basement depth and indicates that the main fault forming the northern basin margin is located close to the southern end of profile 7. A more gradual southward increase in basement depth is suggested by profile 5. The trough in the TMI curve at profile meter 1500 may indicate a fault. The positive anomaly in the north of profile 1 is best matched by two adjacent bodies with susceptibilities of 0.004 and 0.009, respectively.

Structural investigations

Methods

A digital elevation model (DEM) was used to map linear morphological features likely to depict brittle faults, and to reveal the geometry of major structures, which cannot be mapped in the field due to limited and poor outcrops in the basin and along its margins. The DEM is shown in Fig. 10a as a shaded relief map illuminated from the north-west. The azimuth and length of 244 linear features were identified and the azimuthal distribution of the structures, weighted for their length, is presented in a rose diagram (Fig. 10b).

The interpretations are supported and controlled by structural field analyses of microtectonic data collected in 21 outcrops, which were performed to assess the geometry and mechanics of the mapped faults. Brittle structural data were collected from drilling cores from Miocene rocks and outcrops in the pre-Miocene basement. Unfortunately, none of the few outcrops of Miocene rocks provided tectonic information. For kinematic analysis in carbonate rocks extension gashes, stylolithes, fibrous calcite and s-planes within the fault gauge were analysed. Fibrous slickensides and Riedel planes were found in phyllites and metavolcanites. Separation of field data into homogeneous data sets was based on field observations

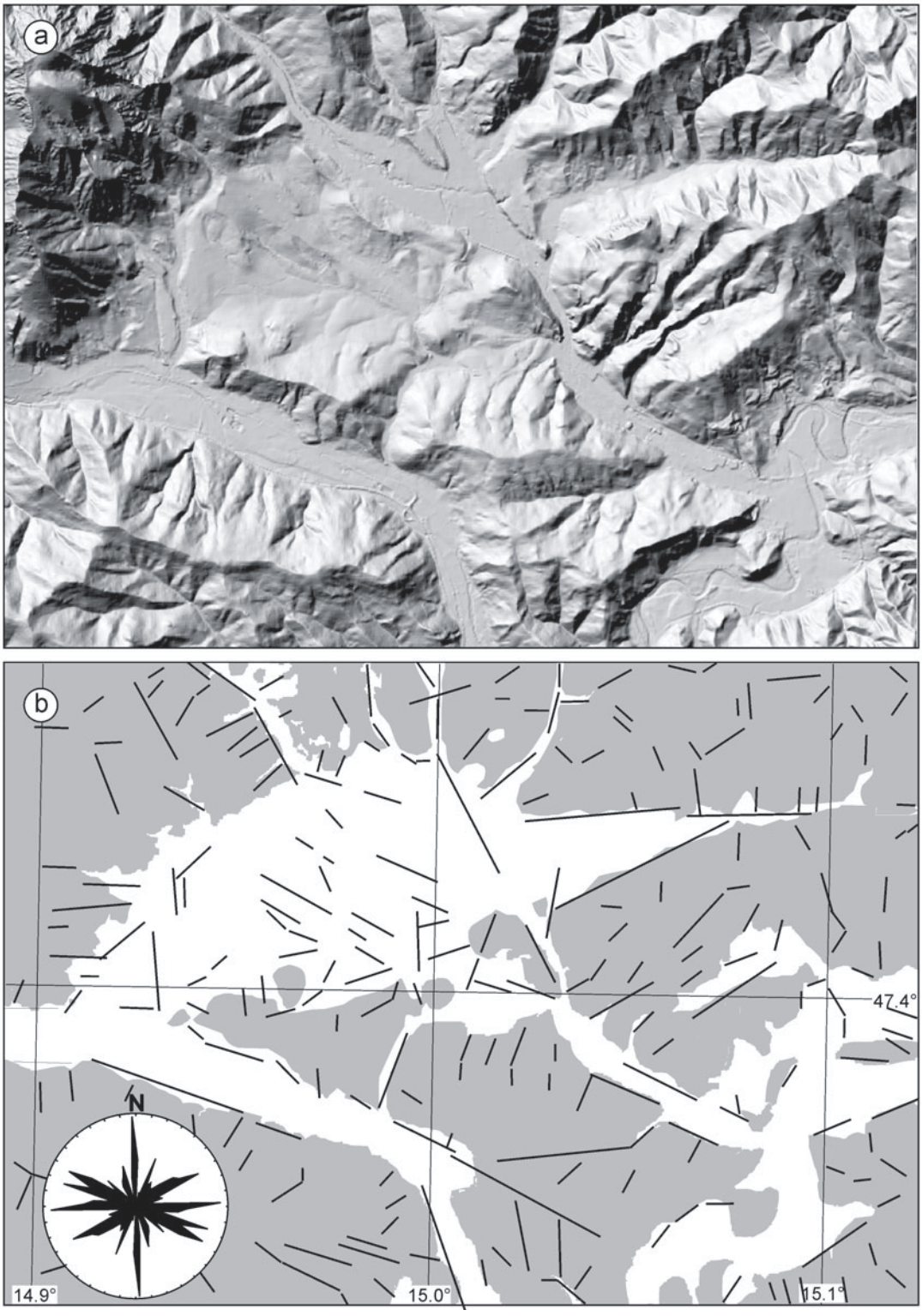

Fig. 10. a — Digital elevation model (DEM) of the study area. **b** — Interpretation of DEM and trend distribution of traces added in rose diagram.

of the relative chronology of deformational events. Bending of striation, superimposed striations on fault surfaces as well as cross-cutting relationships between faults were used for establishing this chronology. The homogeneity of separated data sets was checked by the computation of pT-axes (Turner 1953). The results were plotted in stereographic projections of fault patterns in Schmidt net, lower hemisphere.

Interpretation

In the rose diagram (Fig. 10b) several groups of lineament-directions can be identified. In the first part of this section, E–W to NE–SW striking faults which form the margins of the Trofaiach Basin are discussed. Microstructural data from these faults are plotted in Fig. 11.

An important group of morphological lineaments trends roughly W–E (ca. 265–085). The map-scale Trofaiach Fault in the Laintal area is one of these lineaments. Microstructural data are not available from the Trofaiach Fault in the Laintal area because of bad outcrops. However, Nievoll (1985) found ample evidence for sinistral movements along the central and eastern sector of the 30 km long fault. Evidence for sinistral strike-slip faulting is also present at the margins of the Trofaiach Basin, where a displaced thrust fault indicates displacements in the order of 10 km (Fig. 11). This distance roughly agrees with Vetters' (1911) estimate, which reconstructed a displacement of 12 km along the central Trofaiach Fault. West of Trofaiach, the Trofaiach Fault is hidden, but gravimetric data suggest a 4 km continuation westwards (Fig. 6b). The main structure of the Trofaiach Fault is not exposed, but accompanying minor faults show cataclasite and reddish or brownish kakirite. Left lateral W–E trending lineaments also form important structures with duplexes in carbonates along the southern part of the western basin margin (Fig. 10; sites 13–18 in Fig. 11). The W–E directed lineaments are not observed within the Trofaiach Basin, where they are covered by Miocene rocks.

A second group of lineaments strikes ca. WSW–ENE (235–055 to 255–075; Fig. 10). Left-lateral faults in this group are mostly interpreted as Riedel shears of the sinistral Trofaiach Fault, formed during the initial stage of basin formation. Representative faults are excellently exposed in a quarry north of Trofaiach (site 1; Fig. 11). Other representatives of this group are found in the south-eastern margin of the Trofaiach Basin (see also Figs. 7, 9). In the Laintal area, limestone along the fault is covered by a massive fault breccia. In the south-western basin two branches of the strike-slip fault confine an eastward tilted basement wedge. Numerous small scale WSW–ENE to W–E directed strike-slip faults and dip-slip faults run parallel to the main structure. Some outcrops show small scarps, others up to 1 m thick brownish kakirite and cataclasite. Sinistral faults are also documented in Miocene sediments drilled from the boreholes KB1–2 and A5 (Fig. 3). As the cores are not oriented, the direction of sinistral strike-slip movements cannot be safely determined. However, the predominance of WSW-trending lineaments within the south-

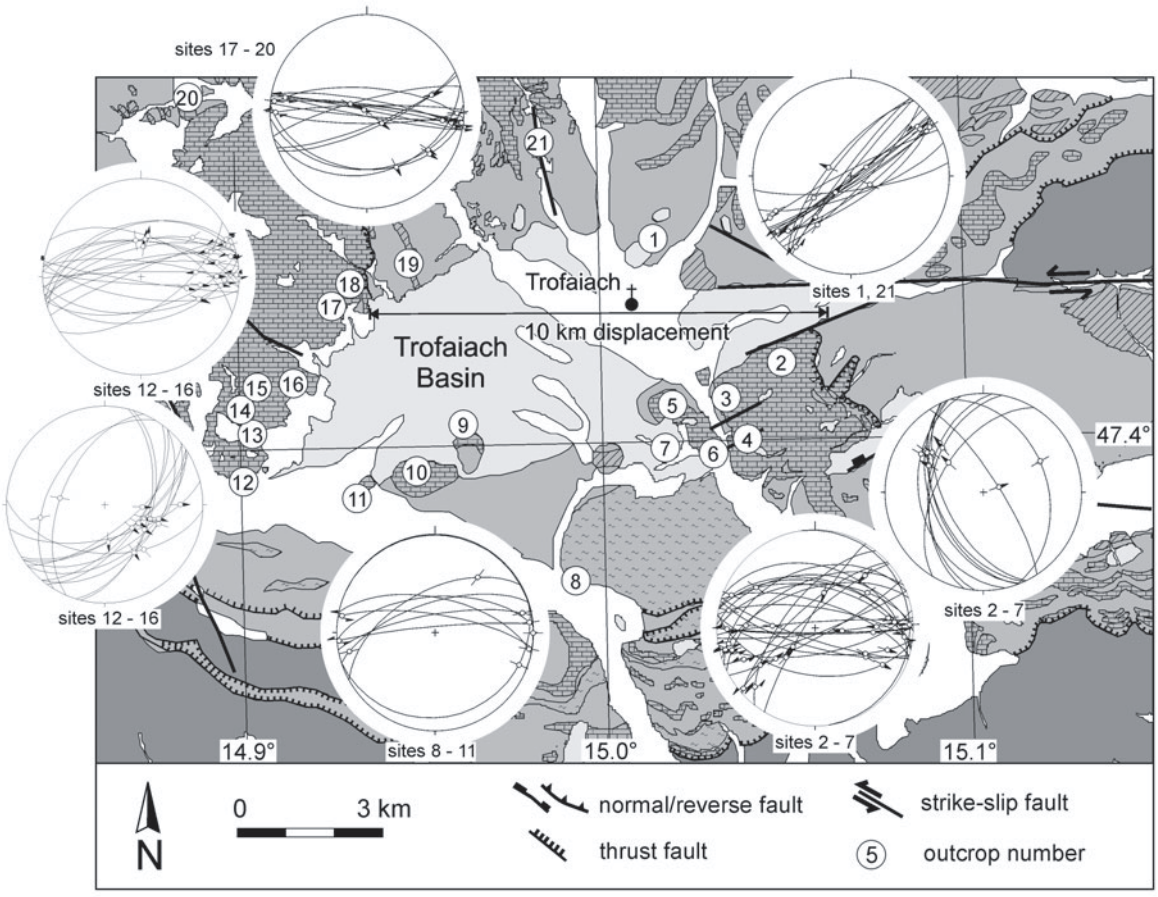

Fig. 11. Selected tectonic data for the pull-apart phase of the Trofaiach Basin. Fault planes are plotted in Schmid net, lower hemisphere projection. Great circles and points denote fault planes and slicken lines, respectively. Double arrows indicate sense of shear.

ern Trofaiach Basin suggests that the cored faults are related to this group of lineaments. This indicates that the faults remained active after the deposition of the Miocene rocks.

NE-striking lineaments with strike directions between 225–045 and 235–055 occur at the western basin margin (Fig. 10). They coincide with SSE- (sites 17–19) and SE-dipping (sites 12–15) oblique-normal faults (Fig. 11). This pattern suggests that the E–W directed Trofaiach strike-slip fault in the north bends into an oblique-normal fault at the western basin margin. Simultaneously, the NE-striking normal faults are displaced by sinistral E–W trending strike-slip faults.

Whereas the above faults are kinematically and geometrically related to the extensional phase of basin formation within the framework of Miocene lateral extrusion, the role of lineaments discussed below is ambiguous.

A prominent group of morphological lineaments trends 280–100 to 310–130 (Fig. 10) sub-parallel to major valleys. Scarps in the basement west of the Trofaiach Basin, as well as thick kakirites and cataclasites are related to such faults. Although not detectable in geophysical studies, this group forms conspicuous lineaments in the Trofaiach Basin. SE trending faults are frequently observed within the north-eastern Eastern Alps (e.g. Peresson & Decker 1997) and are generally related to Late Eocene/Early Miocene dextral movements. A conjugate sinistral fault system strikes N to NE. During Late Miocene times E-W compression reactivated several of these faults with opposed shear sense (Peresson & Decker 1997). This may explain the observed evidence for both sinistral (e.g. sites 6, 7) and dextral (sites 14–16, 19) SE trending faults within the basement rocks (Fig. 12). Within the Miocene basin fill, dextral NE and sinistral SE trending faults fitting the Late Miocene stress pattern are expected. However, a sketch of the Gimplach mine (Fig. 12) shows dextral SE (~310 to 130) and sinistral NE (200 to 020) trending faults. This fault pattern suggests N-S (NNW–SSE) compression.

Discussion

Basin architecture

The northern margin of the basin is formed by the roughly E-W striking sinistral Trofaiach Fault (Fig. 13). Interpretation of the DEM (Fig. 10) and of the gravimetric (Fig. 6) and magnetic data (Figs. 8, 9) suggests that the fault controlled northern basin margin is split from east to west into three segments, with each western segment slightly displaced towards the north. The exact position of the main fault along magnetic profile 7 (Fig. 9), which crosses the Trofaiach Fault northwest of Trofaiach, is ambiguous. The magnetic survey suggests that the main fault is located at the southern edge of a modelled body, whereas a high gravimetric gradient suggests a slightly more northern position. Changing the relative magnetic susceptibility of the model body (e.g. to 0.024 corresponding to the highest observed value) does not solve the problem. Perhaps there are two faults resulting from the over-

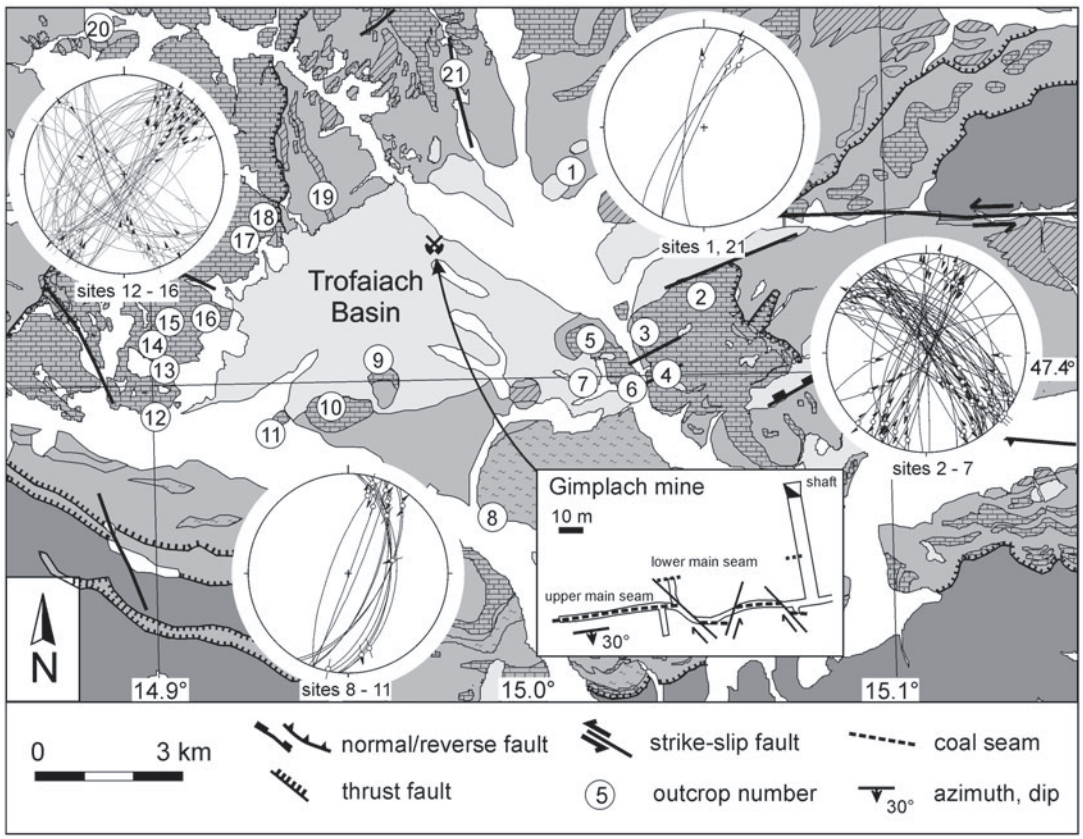

Fig. 12. Selected tectonic data for faults pre- and postdating the main pull-apart phase of the Trofaiach Basin. Fault planes are plotted in Schmid net, lower hemisphere projection. Great circles and points denote fault planes and slicken lines respectively. Double arrows indicate sense of shear. The insert is a sketch map of the fault pattern reported from the Gimplach coal mine.

lap of the western and central segments of the Trofaiach Fault. However, because of thick Quaternary cover this hypothesis cannot be checked. The Trofaiach Fault disappears about 6 km west of Trofaiach. Indications for a westward continuation of the fault exist neither at the northern end of seismic line TR0001, nor within the exposed basement. NW–SE trending sinistral strike-slip faults north of the Trofaiach Fault (e.g. site 1 in Fig. 11) are interpreted as Riedel shears.

The south-eastern basin margin is accompanied by two parallel ENE–WSW striking faults, which include an angle of about 20° with the Trofaiach Fault. The southern fault forms the main southern margin of the basin. This rather straight margin is interrupted by a northward protrusion of basement rocks south of Trofaiach, splitting the basin margin into two sectors. The eastern sector is clearly visible in the DEM. The western sector is visible in the DEM, the gravimetric and the magnetic survey. The seismic line TR0001 shows that the fault comprises several steep branches (fault system 5 in Fig. 5). The northern ENE–WSW striking fault is visible in the gravimetric survey, but its westernmost part is also visible in the DEM. The fault separates Miocene rocks in the north from basement rocks in the south along its western part, and grades eastwards into a steep central basin fault (fault system 4 in Fig. 5). Both parallel faults enclose a basement block, which is tilted towards the ENE.

Gravimetric and structural data suggest that the north-western basin margin is formed by south-eastward dipping normal and oblique-normal faults. These faults are displaced by E–W trending strike-slip faults. Tilted Miocene rocks, but no south-eastward dipping normal faults, are visible at the northern end of seismic line TR0001.

An ENE–WSW striking gravity low is located in the western part of the basin between the Trofaiach Fault, the north-western basin margin and the northern ENE–WSW striking fault (Fig. 13). Traditionally this feature would be interpreted as the depocenter of the basin. However, the model in Fig. 7 suggests that at least at its eastern end, the gravity low may be the result of shallow low density bodies within the basin fill. Along the strike, the axis of the gravity low is laterally displaced.

According to seismic data and the gravity model, the basin depth is in the range of 800 to 900 m. Borehole A5 shows that the preserved thickness of Miocene rocks in the narrow eastern part of the basin in the Laintal area is at least 550 m. This implies steep marginal faults.

Seismic line TR0001 provides information on the internal architecture of the basin. Along the northern part of this line the rocks dip in southward directions (~ 30°) and are horizontal or dip slightly southward along the central and southern part. Southward tilting of the northern part is related to faulting along fault system 2 (see Fig. 5). A major unconformity separates rocks from a lower and an upper complex.

Basin evolution

Inferences about the evolution of the Trofaiach Basin fill based mainly on borehole data (Fig. 3) and on information from seismic line TR0001 (Fig. 5) are presented in this section. However, the reconstruction is fragmented because of the limited availability of sample material and the lack of interpretable reflectance patterns in some parts of the seismic transect. The latter is due at least in part to a result of intense faulting.

Sedimentation in the Trofaiach Basin commenced with the deposition of coarse-grained clastic rocks. Conglomerates were drilled in boreholes Trofaiach 1 and A5 and are also preserved in outcrops north of the Trofaiach Fault. The basal conglomerates in borehole Trofaiach 1 are overlain by coaly and calcareous shale. Seismic patterns along the northern part of line TR0001 suggest that transport directions perpendicular to the seismic line prevailed during the early stages of basin evolution. Coaly shales in Trofaiach 1 and a thin coal seam with sapropelic shale found at the former exploration mine near Baumgartner indicate a shallow lacustrine or a marginal fluvial depositional environment.

Clinoform geometries between seismic reflectors C and D indicate a later deltaic system, which prograded with apparent northern directions into an approximately 50 m deep lake. Sandy layers in borehole Trofaiach 1 at an elevation of 500 m may represent the sandy topmost part of the prograding delta.

The rocks below reflector D are affected by northward dipping faults (fault system 1) south of borehole Trofaiach 1, which were only active during the early phases of basin evolution. Because of poor seismic resolution, the continuation of the rocks south of fault system 1 remains unclear.

The thickness of the tilted Miocene deposits below seismic reflector D is about 250 m. Remarkably, the thickness does not decrease northwards (Fig. 5). This suggests either a steep fault north of seismic line TR0001, which is not observed, or, more likely that the early basin continued northwards across the basin margin which exists today. It cannot be decided whether the Trofaiach Fault was active during these early stages. Tilting of the northern part of the basin occurred after formation of reflector D and resulted in uplift of the pre-Miocene basement along the north(west)ern basin margin, a steep (30°) southward dip of Miocene rocks and significant erosion of these rocks north(west) of the present-day basin margin. The mechanisms which caused this inversion are poorly understood, because no indications for syndepositional compression or transpression (reverse faults or folds) were found in outcrops. In any case, basal Miocene rocks north of Trofaiach are in a horizontal position, indicating that tilting did not occur north of the Trofaiach Fault.

The sedimentary sequence between seismic reflectors D and E is dominated by fine-grained clastic rocks and overlies reflector D with an onlap or with a downlap relation. The thickness of the sedimentary sequence increases southwards and the dip angles decrease upwards (Fig. 5). Both features are consequences of synsedimentary normal faulting along listric fault 2.

Thereafter, major erosion incised a channel-like structure in the central basin. Sand, silt and clay of the upper complex onlap the erosional surface. Cross bedding and local coaly interlayers indicate a fluvio-deltaic facies. Sediments in boreholes KB1–3 are extremely rich in detrital mica. The mica is most probably derived from Middle Australpine micaschists suggesting sediment transport from eastern or southern directions. Displacements of seismic reflector E and steeply dipping normal and strike-slip faults in shallow drillholes KB1–3 testify that faulting continued during and after deposition of upper complex rocks.

Maturity data indicate that the preserved rocks represent only a part of the entire basin fill. Rocks more than 1000 m thick were removed by erosion. This erosion is probably related to compressional events, which affected the Trofaiach Basin during post-Middle Badenian times.

A roughly N-S compressional event fragmented the coal seam in the Gimplach mine (Fig. 12). Similar fault geometries are known from the Fohnsdorf Basin and are related to post-Middle Badenian movements along the Lavanttal Fault (Sachsenhofer et al. 2000; Strauss et al. 2001). On the other hand, the reconstructed compression also agrees with the present-day stress-field (Reinecker & Lenhardt 1999). An additional E-W compressional event is suggested by the en-echelon arrangement of the sectors of the Trofaiach Fault (Fig. 13) which does not fit with Early/Middle Miocene sinistral movements, and by the protrusion of basement rocks at the south-eastern basin margin along dextral NNE and sinistral NW trending faults. The latter event fits well with Late Miocene E-W compression across the Alpine-Pannonian realm (Decker & Peresson 1996; Peresson & Decker 1997).

Basin models

Classical pull-aparts form at major oversteps between discontinuous master faults and at releasing bends on throughgoing faults (Aydin & Nur 1982; Mann et al. 1983; Sylvester 1988). Both mechanisms require the existence of a master fault at both sides of the pull-apart structure. Extensional structures in strike-slip regimes also develop at the end of strike-slip faults (Deng & Zang 1984). In this case the basin subsides along splay faults (Willemse & Pollard 1998) and normal faults generated by extension parallel to the main fault.

The Trofaiach Basin is clearly related to the sinistral Trofaiach Fault. However, a continuation of this fault or a

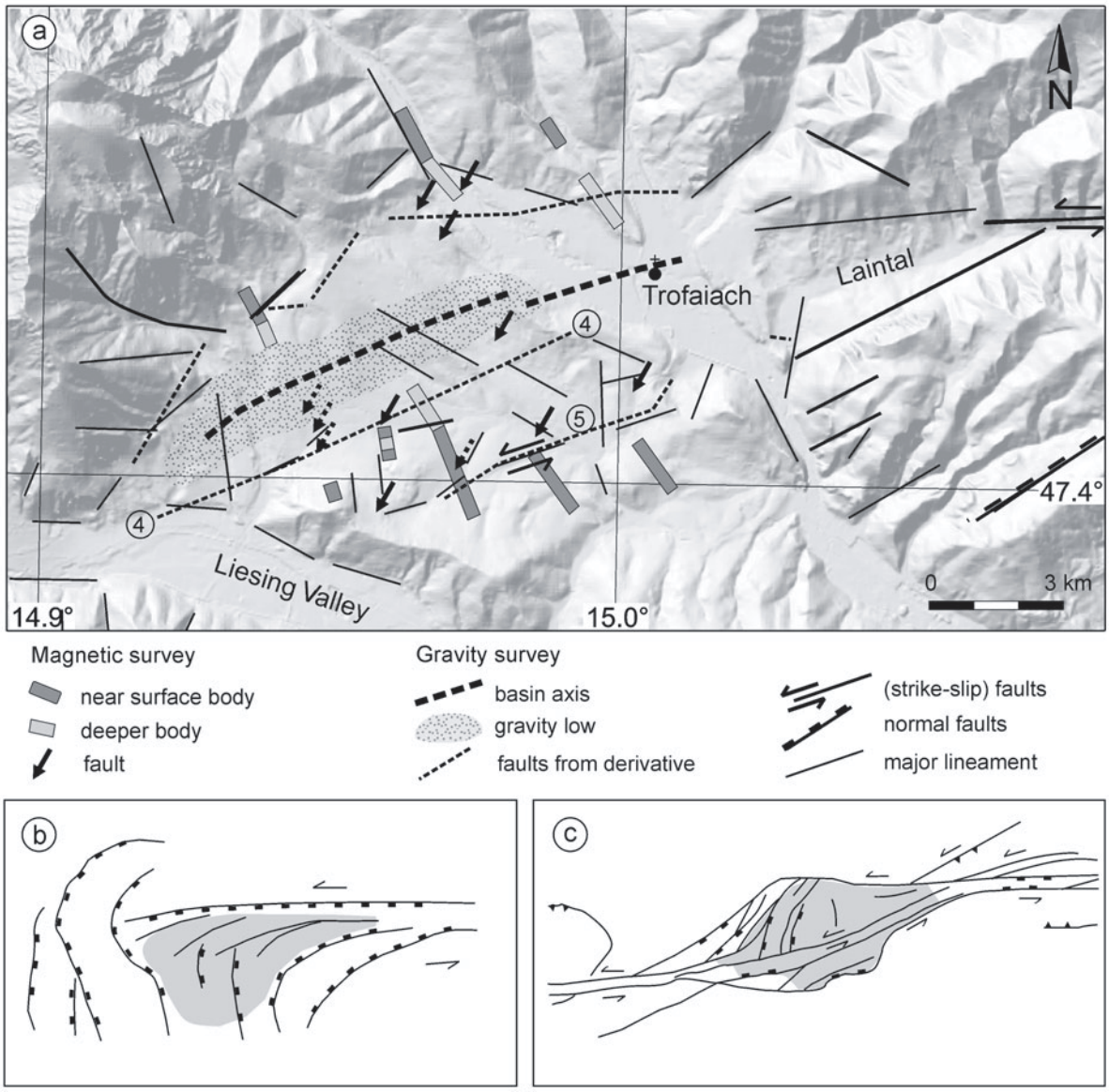

Fig. 13. a — Summary of important features of the Trofaiach Basin derived from geophysical and geological investigations. **b** — Fault pattern at the termination of a single strike-slip fault (modified after a sandbox model; Fig. 7c in Basile & Brun 1999). **c** — Fault pattern at the non-overlapping overstep of two strike-slip faults (modified after a sandbox model; Fig. 10b in Dooley & McClay 1997).

separate master fault at the south-western end of the Trofaiach Basin in the Liesing Valley are not as obvious. Therefore, it was first tested whether the geometry of the Trofaiach Basin can be explained by movements along the Trofaiach Fault alone. Basin formation at the end of a strike-slip fault was modelled by Basile & Brun (1999). Resulting fault patterns are sketched in Fig. 13b. Applied to the Trofaiach Basin, the uplift of basement rocks north-west of the basin and block tilting towards the basin centre could be explained by the formation of a marginal ridge contemporaneous to the horse tail splay at which the adjacent basin subsided. At the western end of the northern branch, strike-slip displacement is partly transferred into NE–SW strike. Such behaviour was also found in the analogue model by Basile & Brun (1999), in outcrop scale (Kim et al. 2001), and on major intraplate strike-slip zones (Storti et al. 2001). However, apart from the north-western basin margin, there is no evidence for E–W trending strike-slip faults bending into N–S directed normal faults. Moreover, about 10 to 14 km of left-lateral motion occurred along the Trofaiach Fault. This was only partly compensated by the formation of the Trofaiach Basin, which is not even 1000 m deep. Thus, most of the strike-slip movement must have passed through the basin and continued in the west. These are major arguments that the Trofaiach Basin represents a classical pull-apart structure.

Possibly, the westward continuation of the Trofaiach Fault is hidden below the Quaternary cover of the generally NW–SE trending Liesing Valley. Sinistral displacements along the Liesing Valley were postulated by Ratschbacher et al. (1991) and Neubauer et al. (1995). Perhaps, a short WNW–ESE trending sector of this valley at the south-western tip of the Trofaiach Basin (Fig. 1) indicates sinistral displacement of the Liesing Valley. Alternatively, younger NW–SE strike-slip movement may have disrupted or overprinted the Trofaiach Fault in the Liesing Valley. Accepting that the Trofaiach Fault continues into the Liesing Valley, the structure of the Trofaiach Basin (Fig. 13a) shows striking similarities to fault patterns found by analogue modelling (Hempton & Neher 1986; Dooley & McClay 1997; Fig. 13c). The similarities include the positions of the main strike-slip faults, which grade into (oblique) normal faults, the array of Riedel shears, and a strike-slip fault crossing the basin, which in the case of the Trofaiach Basin, links the Trofaiach Fault in the north with a (speculative) strike-slip fault in the Liesing Valley. The main movement is probably transferred along this cross-basin fault zone.

Fig. 14 provides a schematic perspective view of the Trofaiach Basin, showing the basin as a pull-apart structure. The second cross-section from below is based on seismic line TR0001. All other sections are more speculative.

Comparison with other basins along the Noric Depression

Basins along the Noric Depression formed as pull-apart basins (Aflenz Basin, Parschlug Basin), as asymmetric pull-

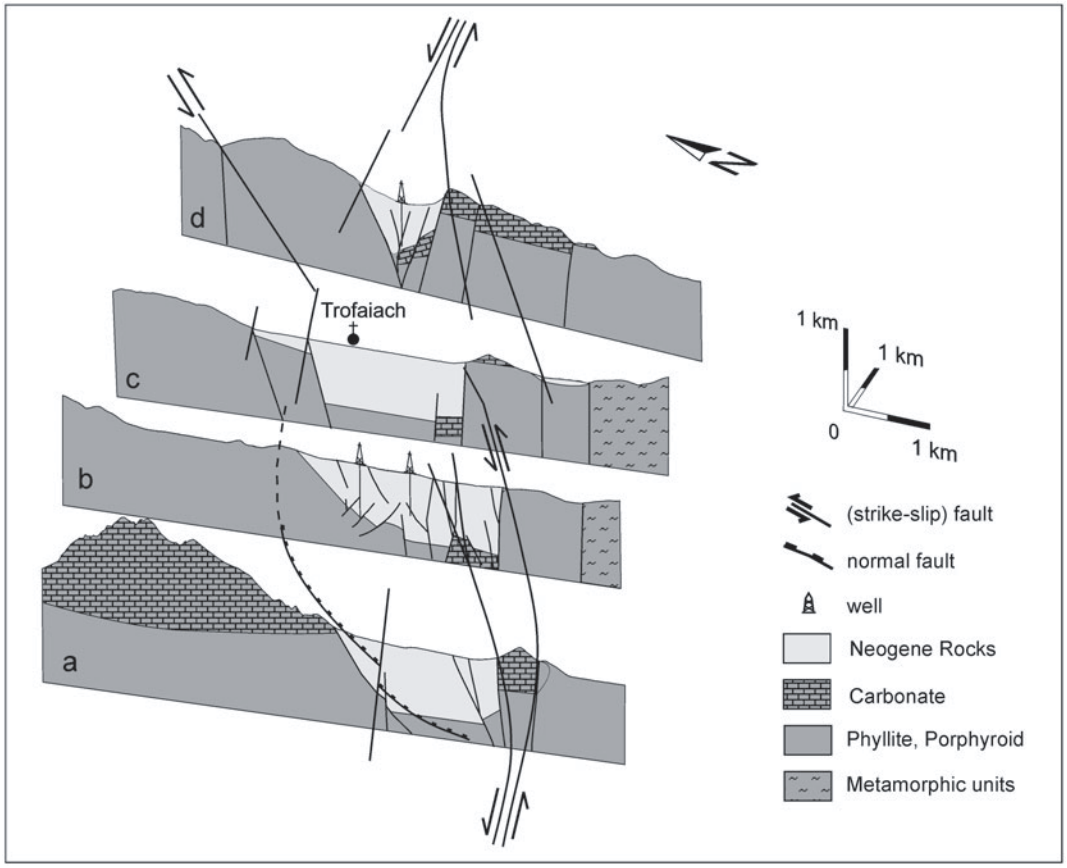

Fig. 14. Perspective view of N-S cross-sections through the Trofaiach Basin. Cross-section 2 is based on seismic line TR0001. The other cross-sections are more speculative.

apart basins (e.g. Leoben Basin), or are characterized by a pull-apart phase and a halfgraben phase (Fohnsdorf Basin; Neubauer et al. 2000; Strauss et al. 2001; see Fig. 1 for location of basins). Despite these differences, the sedimentary sequence of these basins is quite similar and typically comprises (from bottom to top) fluvial sediments, a single thick coal seam, a sapropelite, and fine-grained lacustrine/brackish clastics, which grade upwards into coarse-grained clastic sediments. This sequence reflects very high subsidence rates during the early stages of basin evolution, resulting in the formation of a deep lake and its subsequent filling. Within this framework, the Trofaiach Basin is unique. The basal conglomerates may represent a fluvial phase, and the fine-grained sediments partly represent lacustrine deposits. However, frequent coal layers in different stratigraphic positions indicate that the lake was probably shallow. This is an indication that the subsidence rates in the Trofaiach Basin were smaller than in other basins along the Noric Depression preventing the formation of a deep lake. Subsidence rates in the Trofaich Basin were probably also lower than in the Parschlug Basin, although both basins are controlled by the Trofaiach Fault (Sachsenhofer et al. 2001). Perhaps the lower subsidence rates in the Trofaiach Basin indicate that deposition of the preserved sediments in the Trofaiach Basin commenced before the main faulting activity.

Another difference concerns the development of a cross-basin fault zone in the Trofaiach Basin, which is not apparent in other basins along the Noric Depression. For example, seismic lines in the Fohnsdorf and Aflenz Basins (Sachsenhofer et al. 2000; Gruber et al. 2002) show that faulting in these basins was restricted to the basin margins. This probably reflects differences in strike-slip displacements along the principle fault zone. The overall displacement is about 4 km in the case of the relatively large Fohnsdorf Basin (Strauss et al. 2001), probably even less in the Aflenz Basin, and 10 to 14 km in the Trofaiach Basin. We speculate that only in the Trofaiach Basin an important part of the total displacement had to be transferred along a cross-basin fault zone.

Most basins in the western and central Noric Depression, including the Trofaiach Basin are controlled by E–W trending faults. ENE–WSW trending faults, which are postulated by classical escape models, dominate only in the eastern Noric Depression.

Conclusions

The Trofaiach Basin formed during the Early/Middle Miocene lateral extrusion of the eastern parts of the Eastern Alps at the western termination of the sinistral Trofaiach Fault. The basin geometry suggests that it represents a classical pull-apart structure. It occupies a left step between the Trofaiach Fault with 10 to 14 km of total displacement and a (poorly constrained) strike-slip fault in the Liesing Valley.

The basin is bordered in the north by en-echelon segments of the Trofaiach Fault and in the south(east) by near-vertical ENE–WSW trending faults. The western basin margin is formed by NE–SW trending (oblique) normal faults. Total displacement along the Trofaiach Fault was only partly compensated by basin formation. Part of the displacement was transferred along a cross-basin fault.

The western Trofaiach Basin is about 800 to 900 m deep. Basin depth in the narrow Laintal area exceeds 550 m. According to borehole data and seismic facies, the basin fill is dominated by fluvial and shallow lacustrine deposits. As far as it can be reconstructed, the water depth only reached a maximum of 50 m. In contrast to other basins along the Noric Depression, deep lacustrine environments were not established, indicating that subsidence rates in the Trofaiach Basin were probably lower than in other basins along the Noric Depression. A major erosional unconformity (seismic reflector E) within the basin fill separates a lower complex from an upper complex.

The preserved basin fill represents only part of the original deposits. At least three erosional events occurred during the evolution of the Trofaiach Basin. A first phase is related to tilting of the northern part of the basin along transect TR0001 and uplift of basement rocks north-west of the basin. A deep channel-like structure was eroded into lower complex sediments during a second erosional event. Finally, rocks more than 1 km thick were removed during a third phase. The latter event is related either to post-Middle Badenian N-S or to Late Miocene E-W compression.

The main differences from other basins along the Noric Depression include the presence of a cross-basin fault, more erosional events, coaly layers within the entire basin fill, and the absence of deep lacustrine depositional environments. This shows that basin forming mechanisms changed significantly along different segments of the main wrench corridor within the Eastern Alps.

Acknowledgments: We wish to thank the seismic field crew for their encouragement and the colleagues at Joanneum Research for critical comments on seismic processing and interpretation. We are grateful to G. Walach sen. for supervising the gravity survey and to R. Scholger who helped interpret magnetic data. D. Reischenbacher is acknowledged for cheerfully supporting field work. I. Dunkl kindly provided unpublished FT ages. Linguistic improvement introduced to the manuscript by Ch. Wohlfahrt is also gratefully acknowledged. This study was funded under Grant P 14025-Tec by the Austrian Science Foundation. Parts of the seismic survey were funded by VALL.

References

Aydin A. & Nur A. 1982: Evolution of pull-apart basins and their scale independence. *Tectonics* 1, 91–105.

Basile C. & Brun J.P. 1999: Transtensional faulting patterns ranging from pull–apart basins to transform continental margins: an experimental investigation. *J. Struct. Geol.* 21, 1, 23–37.

Benson A.K. & Mustoe N.B. 1995: Analyzing shallow faulting at a site in the Wasatch fault zone, Utah, USA, by integrating seismic, gravity, magnetic, and trench data. *Engng Geol.* 40, 3–4, 139–156.

Decker K. & Peresson H. 1996: Tertiary kinematics in the Alpine-Carpathian-Pannonian system: links between thrusting, transform faulting and crustal extension. In: Wessely G. & Liebl W. (Eds.): Oil and gas in Alpidic thrustbelts and basins of

Central and Eastern Europe. *EAGE Spec. Publ.* 5, 69–77.
Deng Q. & Zhang P. 1984: Research on the geometry of shear fracture zones. *J. Geophys. Res.* 89, 5699–5710.
Dooley T. & McClay K. 1997: Analog modelling of pull-apart basins. *AAPG Bull.* 81, 11, 1804–1826.
Gruber W., Decker K., Reischenbacher D. & Sachsenhofer R.F. 2002: Beckenarchitektur in der zentralen Norischen Senke. *PanGeo-Abstracts*, Salzburg.
Hempton M.R. & Neher K. 1986: Experimental fracture, strain and subsidence patterns over en-echelon strike-slip faults: implications for the structural evolution of pull-apart basins. *J. Struct. Geol.* 8, 597–605.
Hoefer H. 1902a: I. Bohrung — Eine Bohrung im Muldentiefsten des Tertiärbeckens bei Trofaiach. *Unpubl. report, District Mining Office,* Leoben, 1–3.
Hoefer H. 1902b: Beurteilung des Bohrlochs Nr. 2 bei Trofaiach. *Unpubl. report, District Mining Office,* Leoben, 1–3.
Hussain A. & Walach G. 1980: Subsurface gravity measurements in a deep intra-Alpine Tertiary basin. *Geoexploration* 18, 165–175.
Kim Y.S., Andrews J.R. & Sanderson D.J. 2001: Reactivated strike-slip faults: examples from north Cornwall, UK. *Tectonophysics* 340, 73–194.
Lackenschweiger H. 1951: Bohrung A5 Laintal — Einstellungs- und Abschlußbericht. *Unpubl. report, Geol. B.–A. Vienna,* 1–2.
Mann P., Hempton M.R., Bradley D.C. & Burke K. 1983: Development of pull-apart basins. *J. Geol.* 91, 529–554.
Metz K., Schmid C., Schmöller R., Ströbl E., Walach G. & Weber F. 1978–1979: Geophysikalische Untersuchungen im Gebiet der Seetaler Alpen–Niedere Tauern–Eisenerzer Alpen. *Mitt. Österr. Geol. Gesell.* 71, 72, 213–259.
Militzer H. & Weber F. 1984: Angewandte Geophysik. Band 1. Gravimetrie und Magnetik. *Springer,* Wien, New York, 127–189.
Neubauer F. 1988: Bau und Entwicklungsgeschichte des Rennfeld-Mugel- und des Gleinalmkristallins. *Abh. Geol. B.–A.*, 42, 1–137.
Neubauer F., Handler R., Hermann S. & Paulus G. 1994: Revised lithostratigraphy and structure of the eastern Greywacke Zone (Eastern Alps). *Mitt. Österr. Geol. Gesell.* 86, 61–74.
Neubauer F., Dallmeyer D.R., Dunkl I. & Schirnik D. 1995: Late Cretaceous exhumation of the metamorphic Gleinalm dome, Eastern Alps: kinematics, cooling history and sedimentary response in a sinistral wrench corridor. *Tectonophysics* 242, 79–98.
Neubauer F., Fritz H., Genser J., Kurz W., Nemes F., Wallbrecher E., Wang X. & Willingshofer E. 2000: Structural evolution within an extruding wedge: model and application to the Alpine-Pannonian system. In: Lehner F.K. & Urai J.L. (Eds.): Aspects of tectonic faulting (Festschrift in Honour of Georg Mandl). *Springer,* Berlin, 141–153.
Nievoll J. 1985: Die bruchhafte Tektonik entlang der Trofaiachlinie (Östliche Zentralalpen, Österreich). *Jb. Geol. B.–A.*, 127, 643–671.
Peresson H. & Decker K. 1997: The Tertiary dynamics of the northern Eastern Alps (Austria): changing palaeostresses in a collisional plate boundary. *Tectonophysics* 272, 2–4, 125–157.
Petrascheck W. 1924: Kohlengeologie der Österreichischen Teilstaaten. VI Braunkohlenlager der österreichischen Alpen. *Berg- u. Hüttenmänn. Mh.* 72, 5–48.
Ratschbacher L., Frisch W., Linzer H.G. & Merle O. 1991: Lateral extrusion in the Eastern Alps, 2. Structural analysis. *Tectonics* 10, 257–271.
Reinecker J. & Lenhardt W.A. 1999: Present-day stress field and deformation in eastern Austria. *Int. J. Earth Sci.* 88, 532–550.
Sachsenhofer R.F. 1989: Das Inkohlungsbild im Jungtertiär der Norischen Senke (Östliche Zentralalpen, Österreich) und seine paläogeothermische Deutung. *Jb. Geol. B.–A.,* 132, 489–505.
Sachsenhofer R.F., Sperl H. & Wagini A. 1996: Structure, developement and hydrocarbon potential of the Styrian Basin. In: Wessely G. & Liebl W. (Eds.): Oil and gas in Alpidic thrustbelts and basins of the Central and Eastern Europe. *EAGE Spec. Publ.* 5, 393–414.
Sachsenhofer R.F. 2001: Syn- and post-collisional heat flow in the Tertiary Eastern Alps. *Int. J. Earth Sci.* 90, 579–592.
Sachsenhofer R.F., Kogler A., Polesný H., Strauss P. & Wagreich M. 2000: The Neogene Fohnsdorf basin: basin formation and basin inversion during lateral extrusion in the Eastern Alps. *Int. J. Earth Sci.* 88, 415–430.
Sachsenhofer R.F., Kuhlemann J. & Reischenbacher D. 2001: Das Miozän der östlichen Norischen Senke. In: G.W. Mandl (Ed.): Arbeitstagung 2001. *Geol. B.–A.,* 135–145.
Storti F., Rossetti F. & Salvini F. 2001: Structural architecture and displacement accommodation mechanisms at the termination of the Priestley Fault, northern Victoria Land, Antarctica. *Tectonophysics* 341, 141–161.
Strauss P., Wagreich M., Decker K. & Sachsenhofer R.F. 2001: Tectonics and sedimentation in the Fohnsdorf-Seckau basin (Miocene, Austria): from a pull-apart basin to a half-graben. *Int. J. Earth Sci.* 90, 549–559.
Sylvester A.G. 1988: Strike slip faults. *GSA Bull.* 100, 1666–1703.
Taylor G.H., Teichmüller M., Davis A., Diessel C.F.K., Littke R. & Robert P. 1998: Organic petrology. *Borntraeger,* Berlin–Stuttgart, 1–704.
Turner F.J. 1953: Nature and dynamic interpretation of deformation lamellae in calcite of three marbles. *Amer. J. Sci.* 251, 276–298.
Vetters H. 1911: Die “Trofaiachlinie”. Ein Beitrag zur Tektonik der nordsteirischen Grauwackenzone. *Verh. Geol. R. A.* 151–172.
Weber L. & Weiss A. 1983: Bergbaugeschichte und Geologie der österreichischen Braunkohlevorkommen. *Arch. Lagerstättenforsch. Geol. B.–A.*, 4, 1–317.
Willemse E.J.M. & Pollard D.D. 1998: On the orientation and patterns of wing cracks and solution surfaces at the tips of a sliding flaw or fault. *J. Geophys. Res.* 103, 2427–2438.
Winter P. 1993: Die Karte der Bouguer-Isanomalen der Steiermark. *Österr. Beiträge zu Meteorologie und Geophysik* 8, 55–68.
Yalcin M.N., Littke R. & Sachsenhofer R.F. 1997: Thermal history of sedimentary basins. In: Welte D.H., Horsfield B. & Baker D.R. (Eds.): Petroleum and basin evolution. *Springer,* Berlin, 73–167.